Research Article | Vol. 30, No. 17 / 15 Aug 2022 / Optics Express 29979
Optics EXPRESS

Nondipole effects in terahetz-pulse-assisted strong-field ionization

DEJAN B. MILOŠEVIĆ[1,2,3,*] AND DINO HABIBOVIĆ[1]

[1]University of Sarajevo, Faculty of Science, Zmaja od Bosne 35, 71000 Sarajevo, Bosnia and Herzegovina
[2]Academy of Sciences and Arts of Bosnia and Herzegovina, Bistrik 7, 71000 Sarajevo, Bosnia and Herzegovina
[3]Max-Born-Institut, Max-Born-Strasse 2a, 12489 Berlin, Germany
*milo@bih.net.ba

Abstract: Nondipole effects in processes assisted by a THz field having the strength of a few MV/cm can be significant due to its long wavelength. We illustrate this for strong-laser-field-induced ionization assisted by a THz field. To this end, we generalize our strong-field-approximation theory so that it includes the first-order term in a $1/c$ expansion of the vector potential. We show that in this case, in addition to a shift of the maximum of the photoelectron momentum distribution, the differential ionization probability as well as the cutoff energy can be significantly increased. For an explanation of these unexpected results we use the saddle-point method adjusted to include nondipole effects.

1. Introduction

Strong-field ionization of atomic and molecular systems by midinfrared laser pulses is currently a hot topic of strong-field physics [1]. We have recently shown that this process is modified in the presence of a terahertz pulse [2,3]. Depending on the time delay between the laser pulse and the THz pulse, the differential ionization probability, as well as the maximum photoelectron kinetic energy, can be significantly increased. For example, with the THz field strength of a few MV/cm, which is experimentally available [4–6], above-threshold ionization (ATI) of Ar atoms by a midinfrared strong laser field can generate photoelectrons with keV energies [3].

In our analysis of the THz-pulse-assisted ATI [2,3] we used our version of the strong-field approximation (SFA) [7,8], adapted to the presence of a THz pulse. Our SFA uses the dipole approximation, which is justified for the laser pulse alone, but may be questionable for a strong THz field due to its long wavelength. More precisely, the influence of nondipole effects can be estimated by the value of the parameter

$$\beta_0 = \frac{U_{\mathrm{pT}}}{2m_e c\omega_{\mathrm{T}}} = 9.8264\,\frac{[E_{0\mathrm{T}}(\mathrm{MV/cm})]^2}{[\nu_{\mathrm{T}}(\mathrm{THz})]^3}, \tag{1}$$

where $U_{\mathrm{pT}} = e^2E_{0\mathrm{T}}^2/(4m_e\omega_{\mathrm{T}}^2)$ is the ponderomotive energy of the electron with mass m_e and charge $-e$ in the presence of the THz field of intensity $I_{\mathrm{T}} = E_{0\mathrm{T}}^2$ and angular frequency $\omega_{\mathrm{T}} = 2\pi\nu_{\mathrm{T}}$ (in the remaining part of the paper we will use atomic units in which $\hbar = m_e = e = 1$ and the velocity of light is $c = 137.036$ a.u.). Physically, the parameter β_0 has the dimension of length and represents the amplitude of the electron motion parallel to the field propagation direction (the so-called figure-eight motion; see [9,10] and references therein; see also recent review article [11]). The shift of the photoelectron momentum distribution along the propagation direction is related to the radiation pressure and has been observed in the experiment with argon and neon atoms, laser wavelength 1400 nm, and intensity $10^{14} - 10^{15}$ W/cm^2 [12] (see [13] for a theoretical analysis). Very recently, nondipole SFA was presented in [14] and applied to detachment of electrons from negative ions by a midinfrared laser field.

#468146 https://doi.org/10.1364/OE.468146
Journal © 2022 Received 17 Jun 2022; revised 20 Jul 2022; accepted 20 Jul 2022; published 1 Aug 2022

Optics EXPRESS

For $\beta_0 \gtrsim 1$ a.u. the dipole approximation is questionable. In Eq. (1) we expressed the field and the frequency in units as they are normally used for the THz field. The analogous formula for the laser intensity I_L and wavelength λ_L is $\beta_0 = 0.027478 I_L(10^{14}\ \mathrm{W/cm^2})[\lambda_L(\mu\mathrm{m})]^3$. In this paper we will use the example of $I_L = 1\times10^{14}$ W/cm^2 and $\lambda_L = 3100$ nm, for which we have $\beta_0 = 0.8186$ a.u.<1 a.u. On the other hand, for the used THz field with $\nu_T = 1$ THz and the field strength $E_{0T} = \{2.838, 5, 10\}$ MV/cm we have $\beta_0 = \{79.1, 246, 983\}$ a.u., so that the dipole approximation is not justified.

In the present paper, in order to explore the nondipole effects introduced by a strong THz pulse, we first introduce our nondipole SFA in Sec. 2. In Sec. 3. we present our numerical results. We first define our combined laser and THz pulse and then present our results for the photoelectron spectra and momentum distributions. Our conclusions are given in Sec. 4.

2. Improved SFA with nondipole corrections

The improved SFA, formulated in [7] for an elliptically polarized few-cycle laser pulse, can be generalized to include nondipole effects. The main idea is to expand vector potential, which is a function of $\omega t - \mathbf{k}\cdot\mathbf{r} = \omega(t - \hat{\mathbf{k}}\cdot\mathbf{r}/c)$ (ω is the angular frequency and $\mathbf{k}$ is the wave vector with $\hat{\mathbf{k}}$ the unit vector), in powers of $1/c$. This leads to the replacement of the vector potential in dipole approximation $\mathbf{A}(t)$ by $\mathbf{A}(t) + \frac{\hat{\mathbf{k}}\cdot\mathbf{r}}{c}\mathbf{E}(t)$, with $\mathbf{E}(t) = -d\mathbf{A}(t)/dt$ the electric field vector. Consequently, the dipole interaction $\mathbf{E}(t)\cdot\mathbf{r}$ is replaced by the operator [15]

$$H_I(t) = \mathbf{E}(t)\cdot\left(\mathbf{r} - i\frac{\hat{\mathbf{k}}\cdot\mathbf{r}}{c}\frac{\partial}{\partial\mathbf{r}}\right). \tag{2}$$

The Volkov state of an electron with the momentum $\mathbf{p}$, used in the improved SFA, is replaced by the nodipole Volkov state

$$\begin{aligned} |\chi_{\mathbf{p}}(t)\rangle =& |\mathbf{P}_{\mathbf{p}}(t)\rangle e^{-iS_{\mathbf{p}}(t)}, \quad S_{\mathbf{p}}(t) = \frac{1}{2}\int^t dt' \mathbf{P}^2_{\mathbf{p}}(t'), \\ \mathbf{P}_{\mathbf{p}}(t) =& \mathbf{p} + \mathbf{A}(t) + \frac{\hat{\mathbf{k}}}{c}\left[\mathbf{p}\cdot\mathbf{A}(t) + \frac{1}{2}\mathbf{A}^2(t)\right], \\ S_{\mathbf{p}}(t) =& E_{\mathbf{p}}t + [\mathbf{p}\cdot\boldsymbol{\alpha}(t) + \mathcal{U}(t)]\left(1 + \mathbf{p}\cdot\hat{\mathbf{k}}/c\right), \end{aligned} \tag{3}$$

where $\mathbf{A}(t) = d\boldsymbol{\alpha}(t)/dt$, $\mathcal{U}(t) = \int^t dt'\mathbf{A}^2(t')/2 = U_p t + \mathcal{U}_1(t)$, and $E_{\mathbf{p}} = \mathbf{p}^2/2$. The nondipole improved SFA can be derived analogously as dipole improved SFA in [7]. The result for the ionization probability amplitude from the ground state $|\psi_0\rangle$ is

$$\begin{aligned} M^{(0)}_{\mathbf{p}} =& -i\int_0^{T_p} dt \langle \mathbf{P}_{\tilde{\mathbf{p}}}(t)|H_I(t)|\psi_0\rangle e^{iS_{I_p\tilde{\mathbf{p}}}(t)}, \\ S_{I_p\tilde{\mathbf{p}}}(t) =& I_p t + S_{\tilde{\mathbf{p}}}(t), \quad \tilde{\mathbf{p}} = \mathbf{p} - \mathbf{A}(T_p), \end{aligned} \tag{4}$$

$$\begin{aligned} M^{(1F)}_{\mathbf{p}} =& -\int_0^{T_p} dt e^{iS_{I_p\tilde{\mathbf{p}}}(t)}\int_0^t d\tau\left(\frac{2\pi}{i\tau}\right)^{3/2} e^{-iS(\mathbf{K}_s;t,\tau)} \\ & \times \langle \tilde{\mathbf{p}} + \tilde{\mathbf{p}}\cdot\mathbf{A}(t)\hat{\mathbf{k}}/c|V|\mathbf{K}_s + \mathbf{K}_s\cdot\mathbf{A}(t)\hat{\mathbf{k}}/c\rangle \\ & \times \langle \mathbf{P}_{\mathbf{K}_s}(t-\tau)|H_I(t-\tau)|\psi_0\rangle, \end{aligned} \tag{5}$$

where I_p is the ionization potential, $V(r)$ is the rescattering potential, T_p is the pulse duration time,

$$\begin{aligned} S(\mathbf{K};t,\tau) =& \int_{t-\tau}^t dt'\left[\mathbf{P}^2_{\mathbf{K}}(t')/2 + I_p\right] \\ =& (E_{\mathbf{K}} + I_p)\tau + \left\{\mathbf{K}\cdot[\boldsymbol{\alpha}(t) - \boldsymbol{\alpha}(t-\tau)] + U_p\tau \right. \\ & \left. + \mathcal{U}_1(t) - \mathcal{U}_1(t-\tau)\right\}(1 + \hat{\mathbf{k}}\cdot\mathbf{K}/c), \end{aligned} \tag{6}$$

Optics EXPRESS

and the stationary momentum, determined by the condition $\partial S(\mathbf{K};t,\tau)/\partial\mathbf{K}=\mathbf{0}$, is [16]

$$\begin{aligned}\mathbf{K}_s =&\mathbf{k}_s+\kappa(\tau)\hat{\mathbf{k}}/c,\quad \mathbf{k}_s=-[\boldsymbol{\alpha}(t)-\boldsymbol{\alpha}(t-\tau)]/\tau,\\ \kappa(\tau) =&\mathbf{k}_s^2-[\mathcal{U}_1(t)-\mathcal{U}_1(t-\tau)]/\tau-U_\mathrm{p}.\end{aligned}\tag{7}$$

The amplitude $M_\mathbf{p}^{(0)}$ describes the so-called direct electrons which, after ionization, do not interact with the core potential, while the amplitude $M_\mathbf{p}^{(1F)}$ describes the rescattered electrons which, after the ionization at the time $t-\tau$, undergo one interaction with the potential $V(r)$ at the rescattering time t.

3. Numerical results

We assume that the electric-field vector is $\mathbf{E}(t)=\mathbf{E}_\mathrm{L}(t)+\mathbf{E}_\mathrm{T}(t+\Delta t)$, where Δt is the time delay between the pulses and

$$\mathbf{E}_J(t)=E_{0J}\sin^2\left[\omega_J t/(2n_{\mathrm{p}J})\right]\cos(\omega_J t+\phi_J)\hat{\mathbf{e}}_x\tag{8}$$

are linearly polarized few-cycle sine-square laser ($J=\mathrm{L}$) and THz ($J=\mathrm{T}$) pulses, with ϕ_J the carrier-envelope phase, $\hat{\mathbf{e}}_x$ the unit vector along the polarization axis, and the pulse duration $T_{\mathrm{p}J}=n_{\mathrm{p}J}T_J$, $T_J=2\pi/\omega_J$, $n_{\mathrm{p}J}$ integer, ω_J angular frequency. The ionization happens only during the much stronger laser pulse, i.e., for $t\in[0,T_\mathrm{pL}]$. The THz pulse, which is turned on at $t=-\Delta t$ and turned off at $T_\mathrm{pT}-\Delta t$, is not strong enough to induce ionization.

We consider ionization of Ar atoms ($I_\mathrm{p}=15.76$ eV) by a 6-cycle sine-square laser pulse of intensity 1×10^{14} W/cm^2 and wavelength 3100 nm, assisted by a 2-cycle sine-square 1-THz pulse with the strength up to 10 MV/cm. For these parameters the time delay is fixed to $\Delta t=120T_\mathrm{L}$ so that a maximum ionization probability and a maximum photoelectron energy are expected, according to the results of Refs. [2,3]. The corresponding vector potentials for the THz field strength such that $A_{0\mathrm{T}}=A_{0\mathrm{L}}$ ($E_{0\mathrm{T}}=2.838$ MV/cm) and for the maximal considered strength $E_{0\mathrm{T}}=10$ MV/ cm are presented in Fig. 1.

We present numerical results obtained using our improved SFA theory with and without taking into account nondipole effects. In addition, in order to explain these results obtained by numerical integration, we use a classical model and the saddle-point method from Ref. [2]. The laser and THz pulses are defined in the xy plane (in all our calculations we assume a linearly polarized field along the x axis, but the method we are using is applicable to arbitrary polarization). We choose the z axis as the quantization axis of Ar atoms. Since the corresponding orbital quantum number is $\ell=1$, we calculate $W_\mathbf{p}=2p\sum_{m=-\ell}^{\ell}|M_{\mathbf{p},\ell m}|^2$ [8]. In the nondipole case all terms $m=-1,0,1$ contribute, while in the dipole case, for our choice of the quantization axis, the term $m=0$ does not contribute (the results do not depend on the choice of the quantization axis; for example, for a different choice of the x axis as the quantization axis the $m=0$ term is dominant, but the result for the summed differential ionization probability is the same). The electrons are emitted in the direction (θ,ϕ), with the fixed angle $\phi=0$ [xz plane; we use the spherical coordinates (p,θ,ϕ)]. Most calculations are done for $\theta=90°$, i.e., for electrons emitted in the polarization direction.

In Fig. 2 we present the differential ionization probability for direct electrons $W_\mathbf{p}^{(0)}$ for emission in the polarization direction $(\theta,\phi)=(90°,0°)$ as a function of the photoelectron kinetic energy in units of the laser-field ponderomotive energy U_pL. The spectrum in the absence of the THz pulse has a well-known cutoff at $2U_\mathrm{pL}$ (cyan line). In the presence of the THz pulse, for the chosen time delay as in Fig. 2, the ionization probability increases and the photoelectron energy spectrum extends to much higher energies. With the increase of the THz field strength $E_{0\mathrm{T}}$ the difference between the dipole and nondipole results becomes more visible (compare blue and magenta lines for $E_{0\mathrm{T}}=10$ MV/cm).

Using the classical model presented in Ref. [2], we can explain the positions of the cutoffs in Fig. 2. In Fig. 3 we present classical results for the maximum photoelectron kinetic energy in

Optics EXPRESS

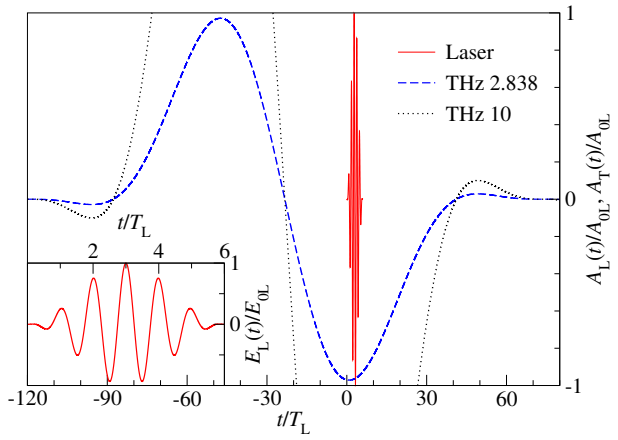

Fig. 1. Linearly polarized sine-square 6-cycle laser and 2-cycle THz pulses with the zero carrier-envelope phases and the time delay $\Delta t = 120T_L$. Inset shows the laser electric field. The corresponding vector potential is presented in the main panel by the red solid line. Laser intensity and wavelength are 1×10^{14} W/cm^2 and 3100 nm, respectively, while the wavelength of the THz field is 300 μm (this corresponds to 1 THz). The vector potential of the THz pulse is shown for the two strength: $E_{0T} = 2.838$ MV/cm (such that $A_{0T} = A_{0L}$ but $I_{0T} = 0.000107I_{0L}$; blue dashed line) and $E_{0T} = 10$ MV/cm ($A_{0T} = 3.52A_{0L}$, $I_{0T} = 0.00133I_{0L}$; black dotted line).

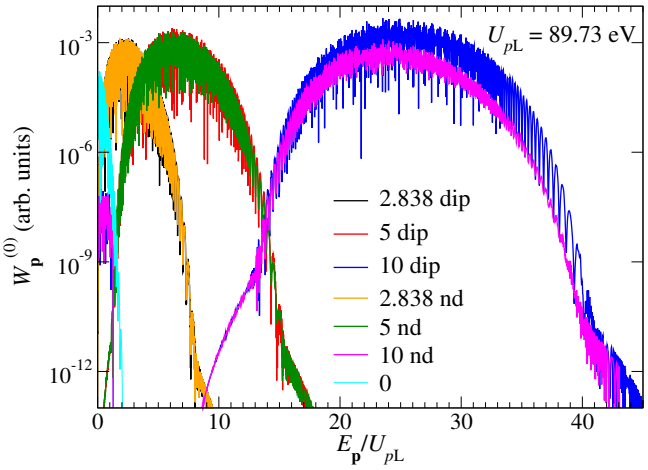

Fig. 2. Differential ionization probability for direct electrons $W_{\mathbf{p}}^{(0)}$ for emission in the polarization direction as a function of the photoelectron kinetic energy for ionization of Ar atoms by the laser pulse alone (cyan line) and by the combined laser and THz pulses with the time delay $\Delta t = 120T_L$. Laser intensity is 1×10^{14} W/cm^2 and the wavelength is 3100 nm. Terahertz field has the frequency 1 THz and the strength 2.838 MV/cm (dipole result - black line, nondipole result - orange line), 5 MV/cm (dipole result - red line, nondipole result - green line), and 10 MV/cm (dipole result - blue line, nondipole result - magenta line).

Optics EXPRESS

units of the laser-field ponderomotive energy $U_{\rm pL}$ as a function of the time delay Δt (in units of the laser-field optical period $T_{\rm L}$) for three different values of the THz field strength and the other laser and THz pulse parameters as in Fig. 2. We see that for $E_{0\rm T} = 2.838$ MV/cm, which corresponds to $U_{\rm pL} = U_{\rm pT}$, the cutoff is above $7.7U_{\rm pL}$ (in comparison with the cutoff position at $2U_{\rm pL}$ in the absence of the THz field). With an increase of $E_{0\rm T}$ the cutoff energy increases and our results shown in Fig. 2 are confirmed (the cutoffs are at $14.7U_{\rm pL}$ and $39U_{\rm pL}$, for 5 and 10 MV/cm, respectively). Therefore, we can use the classical model of Ref. [2] to predict the maximum photoelectron kinetic energy, as well as its dependence on the time delay, which can be useful for future experiments. In Fig. 3 the maximum energy appears for $\Delta t = 70T_{\rm L}$ and $\Delta t = 120T_{\rm L}$. However, only the maximum for $\Delta t = 120T_{\rm L}$ is visible in the results obtained by numerical integration. The maximum for $\Delta t = 70T_{\rm L}$ does not appear. The discrepancy with the classical results can be explained using the quantum-orbit theory [7,8,17–19]. The ionization matrix element can be represented in the form

$$M_{\mathbf{p}} = \sum_s a_s(\mathbf{p}) e^{iS_s(\mathbf{p})}, \tag{9}$$

with the amplitude a_s and the action S_s evaluated at the complex solutions t_s of the saddle-point equation $[\tilde{\mathbf{p}} + \mathbf{A}(t_s)]^2/2 = -I_{\rm p}$. Mathematically, this corresponds to the evaluation of the integral over the time t in Eq. (4) by the saddle-point method (this approximation is valid for large values of the action). However, this result has an important physical meaning which can be understood in terms of Feynman path-integral formalism [18]. The ionization amplitude $M_{\mathbf{p}}$ is expanded in terms of quantum orbits with known spacetime evolution, so that we can review the options available to the electron which is set free by ionization. The fact that the saddle-point solutions and quantum orbits are complex is connected with their origin via the quantum-mechanical process of tunnelling. More precisely, larger is the value of the imaginary part of the time t_s, lower is the ionization probability. We will return to this in the context of Fig. 6. Let us analyze this more carefully for the case of the THz-pulse-assisted ATI for the time delay $\Delta t = 70T_{\rm L}$. The value of the THz vector potential is $A_{\rm T}(t + 70T_{\rm L}) \approx A_{0\rm T}$ and the corresponding saddle-point equation (for $p_z = 0$) takes the form $[p + A_{0\rm T} + A_{\rm L}(t)]^2 = -2I_{\rm p}$, which is the same as that in the absence of the THz field but with the momentum $p' = p + A_{0\rm T}$. Since $p = p' - A_{0\rm T}$, for $p' < A_{0\rm T}$ there are no solutions and the cutoff is much lower than the classical one. On the other hand, $A_{\rm T}(t + 120T_{\rm L}) \approx -A_{0\rm T}$ so that $p = p' + A_{0\rm T}$ and the corresponding cutoff energy is higher than that in the absence of the THz pulse; in this case classical and quantum results agree. Therefore, the time delay Δt is a control parameter which determines the value of $A_{\rm T}(t + \Delta t)$ and thus the ionization probability and the maximum photoelectron energy.

We generalized our code from Refs. [2,3] so that we can calculate photoelectron momentum distributions, both for dipole and nondipole SFA. The corresponding results are presented in Fig. 4. If we compare the results in the absence of the THz pulse (denoted by "0" above the panels) we can see that the nondipole momentum distribution is slightly deformed (it takes the form of parenthesis "(", with the preserved symmetry $p_x \leftrightarrow -p_x$). The reason is that in this case $\beta_0 = 0.8186$ a.u. (for the laser field alone), which is less than one but is not negligible, so that a small difference between the dipole and nondipole results is expected. In the presence of the THz pulse, the momentum distributions obtained using dipole approximation (lower four panels) exhibit the symmetry $p_z \leftrightarrow -p_z$, and the maxima of the distributions are shifted to larger values of p_x for larger values of $E_{0\rm T}$. On the other hand, the nondipole distributions (upper four panels) violate the $p_z \leftrightarrow -p_z$ symmetry, the distributions are slightly deformed, and the position of the maxima in these distributions are shifted to positive values of p_z. This is most noticeable for $E_{0\rm T} = 10$ MV/cm for which we see an additional deformation of the distribution for larger values of p_x and p_z.

For $E_{0\rm T} = 10$ MV/cm the maximum ionization probability is increased by orders of magnitude. Let us explore this unexpected result in more detail. In Fig. 5 we present the photoelectron

Optics EXPRESS

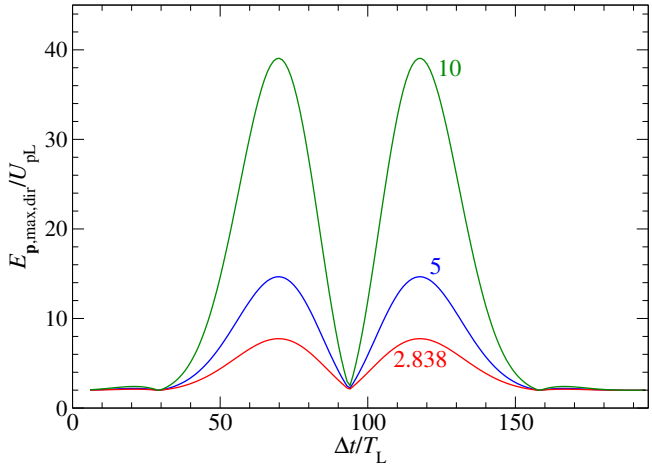

Fig. 3. Maximum photoelectron kinetic energy (in units U_{pL}) as a function of the time delay Δt (in units T_{L}), obtained using classical model from [2]. Laser and THz pulse parameters are as in Fig. 2. The THz field strength in MV/cm is denoted at each curve.

spectra for different emission angles for which, according to Fig. 4, we expect maximal nondipole effects. We see that nondipole differential ionization probability is increased and shifted to higher energies. This is much more pronounced for $E_{0\mathrm{T}} = 10$ MV/cm. As expected, the corresponding dipole results for the angle $\theta = 86.5°$ are suppressed for higher energies.

In order to explain the above unexpected results, we apply the saddle-point method. Using Eqs. (3) and (4) we get that the saddle-point solutions for the complex ionization time are solutions of the nonlinear equation $\partial S_{I_{\mathrm{p}}\tilde{\mathbf{p}}}(t)/\partial t = 0$, which gives

$$p_z^2 + [\tilde{p}_x + A_x(t)]^2 + 2I_{\mathrm{p}} + 2p_z \left[\tilde{p}_x A_x(t) - A_x^2(t)/2\right]/c = 0. \tag{10}$$

In the absence of the THz field, for the laser pulse with $n_{\mathrm{pL}} = 6$ this equation has $2(n_{\mathrm{pL}} + 1) = 14$ solutions [7]. The solutions 5, 6, 7, and 8 in the middle of the pulse give the main contribution to the transition amplitude (9). In Fig. 6 these solutions are presented in the complex ionization time plane for dipole case ($p_z = 0$ and in the absence of the THz pulse; dashed red lines) and nondipole case [$\theta = 87.85°$ and $E_{0\mathrm{T}} = 5$ MV/cm (green circles) and $\theta = 86.5°$ and $E_{0\mathrm{T}} = 10$ MV/cm (black solid lines)]. We see that the curves for $E_{0\mathrm{T}} = 5$ MV/cm and 10 MV/cm have a parabolic shape, while the curves in the absence of the THz field are almost linear. For example, the dashed red line for the solution 5 starts at $\mathrm{Re}\, t \approx 2T_{\mathrm{L}}$ and, with an increase of the energy from $0.01U_{\mathrm{pL}}$ to $50U_{\mathrm{pL}}$, $\mathrm{Im}\, t$ increases from $0.06T_{\mathrm{L}}$ towards $0.38T_{\mathrm{L}}$, while $\mathrm{Re}\, t$ increases towards $2.25T_{\mathrm{L}}$. Since the differential ionization probability exponentially decreases with the increase of $\mathrm{Im}\, t$, the probability which corresponds to this dashed red line becomes negligible for $E_{\mathbf{p}}>2U_{\mathrm{pL}}$ (this agrees with the results presented by cyan line in Fig. 2). On the other hand, due to a parabolic shape of the complex ionization time curve 5 for $E_{0\mathrm{T}} = 5$ MV/cm, the energy in the middle (near $\mathrm{Re}\, t = 2T_{\mathrm{L}}$) is $6.7U_{\mathrm{pL}}$, which explains the results presented by green line in Fig. 2 and by cyan line in Fig. 5 (similar explanation is valid for the solutions 6, 7, and 8, whose contributions interfere, causing oscillations visible in these figures; contribution of the solution 7 is the highest). The values of the energy in units of U_{pL} are denoted by the corresponding color for all three cases: we can follow how the energy changes from zero to $50U_{\mathrm{pL}}$ along the curves.

The maximal differential ionization probability in Fig. 2 is approximately equal for all presented cases. This can be explained comparing the dashed red lines and green circles in Fig. 6: these curves almost overlap and the only difference is in their linear vs. parabolic shapes which explains

Optics EXPRESS

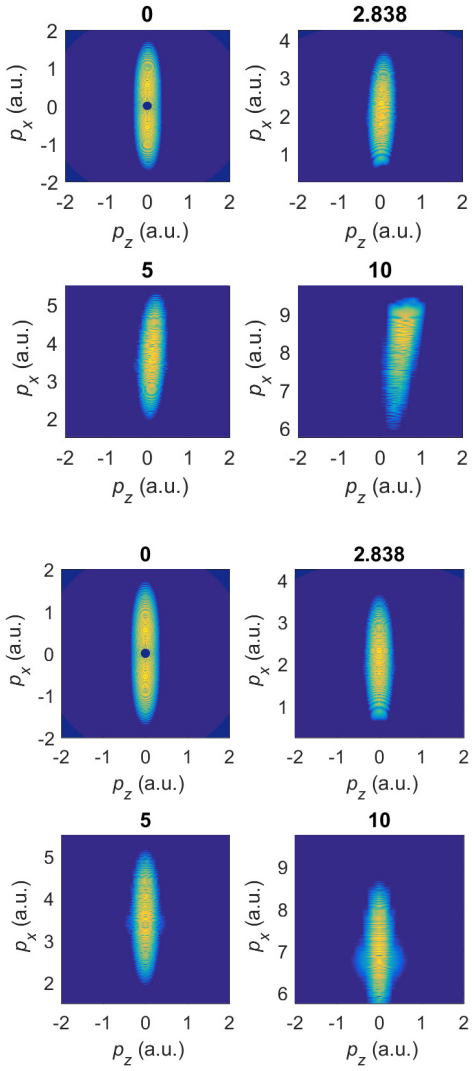

Fig. 4. Photoelectron momentum distributions of direct electrons for ionization of Ar atoms by the combined laser and THz pulses with the parameters of Fig. 2 and the THz field strength (in MV/cm) denoted above each panel. The results in the upper (lower) four panels are obtained taking (not taking) into account nondipole effects. The false color scale covers four orders of magnitude.

much higher electron energies for the $E_{0T} = 5$ MV/cm case, as discussed above. However, in the nondipole case for $E_{0T} = 10$ MV/cm and $\theta = 86.5°$ (green curve in Fig. 5) the differential ionization probability is much higher than in other cases. This can be explained using the corresponding saddle-point complex ionization times presented by black curves in Fig. 6. These curves are shifted down in comparison with the red dashed curves and green circles. The differential ionization probability increases exponentially with the decrease of the imaginary part of the ionization time. As a result, in addition to higher cutoff energies, the differential ionization probability is much higher in this case. Furthermore, the two curves near $\mathrm{Re}\, t = 2.25T_L$ and near $\mathrm{Re}\, t = 3.25T_L$ approach each other which explains the sharp cutoff at $40U_{pL}$ for $E_{0T} = 10$ MV/cm in Fig. 5. Mathematically, the shift down of the above solutions is caused by the last term in

Optics EXPRESS

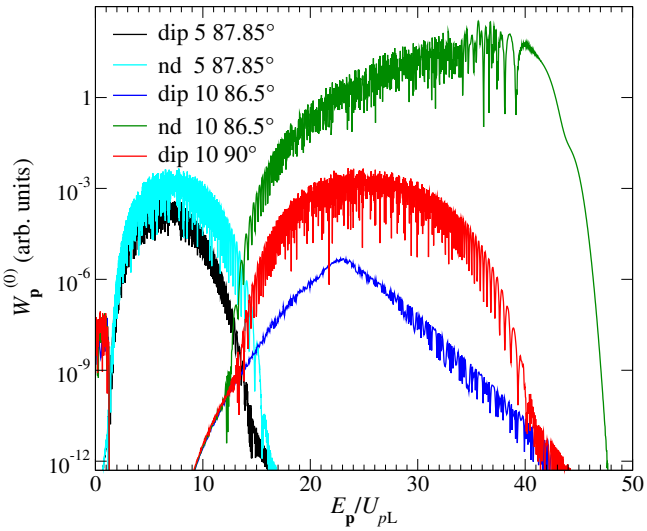

Fig. 5. Differential ionization probability for direct electrons $W_{\mathbf{p}}^{(0)}$ as a function of the photoelectron kinetic energy for the laser and THz pulse parameters as in Fig. 2. In the legend we denote how the calculations are done (dipole SFA "dip" or nondipole SFA "nd"), the THz field strength (5 or 10 MV/cm), and the electron emission angle θ in degrees.

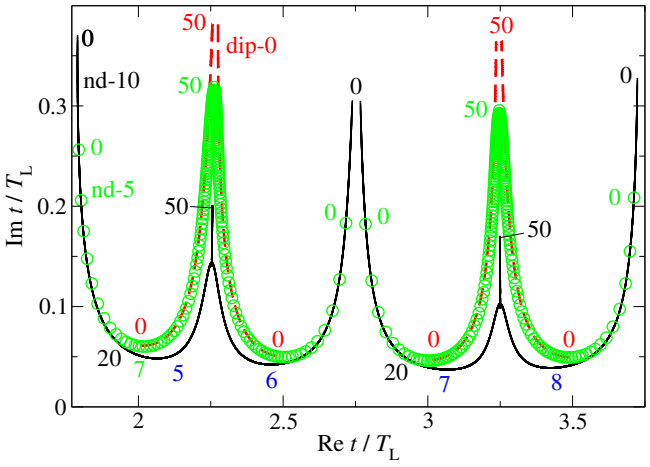

Fig. 6. Direct-electron saddle-point solutions 5, 6, 7, and 8 for the laser and THz pulse parameters as in Fig. 2. Imaginary part of the ionization time is presented as a function of its real part in units of T_{L}. The photoelectron energy changes from $0.01U_{\mathrm{pL}}$ to $50U_{\mathrm{pL}}$ along each curve (particular values of the energy in units of U_{pL} are denoted using the corresponding color). For the results obtained using nondipole saddle-point Eq. (10) and the THz field strength of 5 MV/cm (green circles) and 10 MV/cm (black curves) the electrons are emitted in the direction determined by the angle $\theta = 87.85°$ and $\theta = 86.5°$, respectively. For the case when the THz pulse is absent (red dashed curves) the photoelectrons are emitted in the direction $\boldsymbol{\theta = 90°}$ $\boldsymbol{(p_z = 0)}$.

Optics EXPRESS

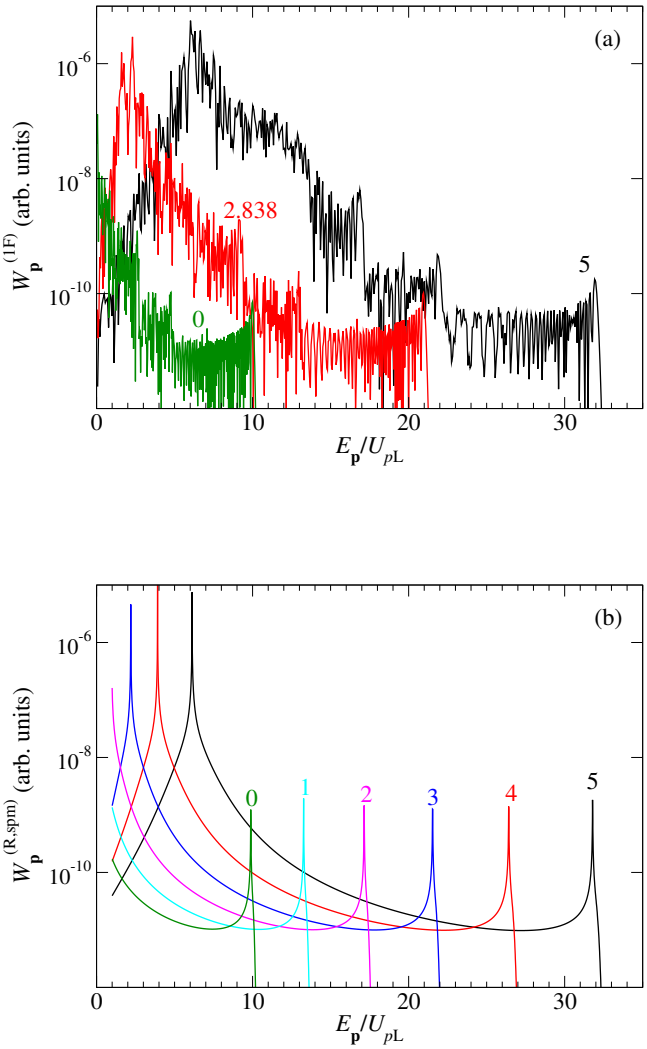

Fig. 7. Differential ionization probability for rescattered electrons obtained using nondipole SFA with numerical integration [(a) $W_{\mathbf{p}}^{(1F)}$] and saddle-point method [(b) $W_{\mathbf{p}}^{(R,spm)}$] for emission in the polarization direction as a function of the photoelectron kinetic energy for ionization of Ar atoms by the laser pulse alone (green line) and by the combined laser and THz pulses with the time delay $\Delta t = 120T_{\mathrm{L}}$. Laser intensity is $I_{\mathrm{L}} = 1 \times 10^{14}$ W/cm^2 and its wavelength is 3100 nm. Terahertz field has the frequency 1 THz and the strength from 1 MV/cm to 5 MV/cm, as denoted above each curve.

Eq. (10) which can become large for strong THz fields. This term is proportional to p_z so that this increase in the differential ionization probability is pronounced for the electrons registered off the polarization axis direction. Physically, in the fashion of Feynman path integral and quantum-orbit formalism [7,8,18], it is the value of the THz vector potential amplitude $A_{\mathrm{T}}(t+\Delta t)$ at the (complex) ionization time t which, for particular time delay Δt, determines both the photoelectron energy and the differential ionization probability [see Eq. (9)].

Finally, in Fig. 7 we present the nondipole SFA results for the rescattered electrons. We see that the cutoff energy increases with the increase of $E_{0\mathrm{T}}$, having a maximum at $32U_{\mathrm{pL}} = 2.87$

Optics EXPRESS

keV for E_{0T} = 5 MV/cm. Applying the saddle-point method to rescattering ionization amplitude, we obtain a system of equations for complex ionization and rescattering times [3,7]. The corresponding differential ionization probabilities, presented in Fig. 7(b), are calculated using only one dominant quantum orbit (for classification of quantum orbits see [8] and references therein; from the pair of short and long orbits which are dominant in the high-energy region we choose the one which is not divergent after the cutoff [3]). We see that the maximum photoelectron energy, i.e., the cutoff position, is reproduced well. Furthermore, for larger values of E_{0T}, in addition to the critical energy at the cutoff, another critical energy (at $6.1U_{pL}$ for E_{0T} = 5 MV/cm) emerges, causing a hump in the spectrum for lower energies. This hump is well reproduced by the numerical results presented in Fig. 7(a). A possible cause of this hump is the shift of the low-energy backward-scattering saddle-point solution [20] towards higher energies with the increase of the THz field strength. Important is that, with the increase of the THz field strength, this hump shifts towards the high-energy part of the spectrum opening the possibility for a more detailed analysis of such structures.

4. Conclusions

In order to explore nondipole effects caused by the long wavelength of the THz field, we generalized our strong-field-ionization theory of the above-threshold ionization assisted by a THz pulse so that it includes corrections due to the first-order term in a $1/c$ expansion of the vector potential. The matrix elements and the action in the nondipole ionization amplitude contain terms in the direction of propagation of the combined laser and THz pulse. As a consequence, the photoelectron momentum distribution is shifted and deformed in comparison with that in the absence of the nondipole effects. Even in the dipole approximation the photoelectron momentum distribution is shifted along the polarization direction in comparison with that in the absence of the THz pulse. This shift is larger for stronger THz fields. If one includes the nondipole effects this distribution is shifted in the pulse propagation direction (i.e., in the p_z direction).

To our surprise, the differential ionization probability can be increased by orders of magnitude due to the presence of the THz pulse. This is explained analysing the behavior of the saddle-point solutions in the complex ionization time plane. The imaginary part of this time is smaller than in the absence of the THz pulse causing, in the fashion of Feynman path integral and quantum-orbit formalism [7,8,18], an increase of the differential ionization probability. Furthermore, the shape of the complex time curve is changed from a linear to a parabolic shape causing the differential ionization probability to be high for much higher energies. This substantial increase of the photoelectron energies to the keV range can also be explained using a classical model. It should also be mentioned that the total ionization probability is not affected by the THz pulse; only the differential ionization probability is redistributed to higher energies due to the influence of the vector potential of the THz field which can be comparable to or larger than that of the laser pulse alone.

It is important to mention that both the strong THz fields [4–6] and the strong 3100-nm laser fields [21] can be realized at the ELI-ALPS facility in Hungary. In addition to the generation of keV photoelectrons, it is important that the process can be controlled by changing the time delay between the THz and laser pulses: the photoelectron spectra can be squeezed or stretched, i.e., the length of the photoelectron spectrum can be shortened or extended. This opens up the possibility of a closer analysis of various low- and high-energy on- and off-axis structures (spider-like and holographic structures, laser-induced electron diffraction, etc. [22–25]; see also the review articles [26,27]). For example, low-energy structures, discovered as a "ionization surprise" in strong-field ionization [28–30] appear at very low energies ($<0.1U_{pL}$) which causes that a precise analysis of these spectra is difficult. However, THz field, depending on the time delay Δt, can extend these structures to higher energies and can increase the corresponding ionization probability. This is a new tool for analysis of the spectra in strong-field physics. An

Optics EXPRESS

example how such structures are extended in the presence of a strong THz field is shown in Fig. 7(b).

Acknowledgments. We acknowledge support by the Ministry of Science, Higher Education and Youth, Canton Sarajevo, Bosnia and Herzegovina, and by the Alexander von Humboldt Foundation, and useful discussions with Wilhelm Becker.

Disclosures. The authors declare no conflicts of interest.

Data availability. Data underlying the results presented in this paper are not publicly available at this time but may be obtained from the authors upon reasonable request.

References

1. B. Wolter, M. G. Pullen, M. Baudisch, M. Sclafani, M. Hemmer, A. Senftleben, C. D. Schröter, J. Ullrich, R. Moshammer, and J. Biegert, "Strong-Field Physics with Mid-IR Fields," Phys. Rev. X **5**(2), 021034 (2015).
2. D. B. Milošević, "Strong-laser-field-induced ionization assisted by a terahertz pulse," Opt. Lett. **47**(7), 1669–1672 (2022).
3. D. B. Milošević, "High-order above-threshold ionization by a few-cycle laser pulse in the presence of a terahertz pulse," Phys. Rev. A **105**(5), 053111 (2022).
4. X. C. Zhang, A. Shkurinov, and Y. Zhang, "Extreme terahertz science," Nat. Photonics **11**(1), 16–18 (2017).
5. D. Matte, N. Chamanara, L. Gingras, L. P. René de Cotret, T. L. Britt, B. J. Siwick, and D. G. Cooke, "Extreme lightwave electron field emission from a nanotip," Phys. Rev. Res. **3**(1), 013137 (2021).
6. L.-G. Zhu, Z. Sheng, H. Schneider, H.-T. Chen, and M. Tani, "Ultrafast phenomena and terahertz waves: introduction," J. Opt. Soc. Am. B **39**(3), UPT1–UPT2 (2022).
7. D. B. Milošević, G. G. Paulus, D. Bauer, and W. Becker, "Above-threshold ionization by few-cycle pulses," J. Phys. B **39**(14), R203–R262 (2006).
8. D. B. Milošević, "Strong-field approximation and quantum orbits," in *Computational strong-field quantum dynamics: Intense Light-Matter Interactions*, edited by D. Bauer, (De Gruyter Textbook, Berlin, 2016), Chap. VII, pp. 199–221.
9. H. R. Reiss, "Limits on Tunneling Theories of Strong-Field Ionization," Phys. Rev. Lett. **101**(4), 043002 (2008); *ibid*. **101**, 159901(E) (2008).
10. H. R. Reiss, "The tunnelling model of laser-induced ionization and its failure at low frequencies," J. Phys. B **47**(20), 204006 (2014).
11. J. Maurer and U. Keller, "Ionization in intense laser fields beyond the electric dipole approximation: concepts, methods, achievements and future directions," J. Phys. B **54**(9), 094001 (2021).
12. C. T. L. Smeenk, L. Arissian, B. Zhou, A. Mysyrowicz, D. M. Villeneuve, A. Staudte, and P. B. Corkum, "Partitioning of the Linear Photon Momentum in Multiphoton Ionization," Phys. Rev. Lett. **106**(19), 193002 (2011).
13. H. R. Reiss, "Relativistic effects in nonrelativistic ionization," Phys. Rev. A **87**(3), 033421 (2013).
14. R. Kahvedžić and S. Gräfe, "Strong-field approximation with leading-order nondipole correction," Phys. Rev. A **105**(6), 063102 (2022).
15. N. J. Kylstra, R. M. Potvliege, and C. J. Joachain, "Photon emission by ions interacting with short intense laser pulses: beyond the dipole approximation," J. Phys. B **34**(3), L55–L61 (2001).
16. C. C. Chirilă, N. J. Kylstra, R. M. Potvliege, and C. J. Joachain, "Nondipole effects in photon emission by laser-driven ions," Phys. Rev. A **66**(6), 063411 (2002).
17. R. Kopold, D. B. Milošević, and W. Becker, "Rescattering Processes for Elliptical Polarization: A Quantum Trajectory Analysis," Phys. Rev. Lett. **84**(17), 3831–3834 (2000).
18. P. Salières, B. Carré, L. Le Déroff, F. Grasbon, G. G. Paulus, H. Walther, R. Kopold, W. Becker, D. B. Milošević, A. Sanpera, and M. Lewenstein, "Feynman's path-integral approach for intense-laser–atom interactions," Science **292**(5518), 902–905 (2001).
19. W. Becker, F. Grasbon, R. Kopold, D. B. Milošević, G. G. Paulus, and H. Walther, "Above-threshold ionization: From classical features to quantum effects," Adv. At., Mol., Opt. Phys. **48**, 35–98 (2002).
20. D. B. Milošević, "Low-energy backscattering quantum orbits in above-threshold ionization," J. Phys. B **49**(17), 175601 (2016).
21. M. Kübel, P. Wustelt, Y. Zhang, S. Skruszewicz, D. Hoff, D. Würzler, H. Kang, D. Zille, D. Adolph, G. G. Paulus, A. M. Sayler, M. Dumergue, A. Nayak, R. Flender, L. Haizer, M. Kurucz, B. Kiss, S. Kühn, B. Fetić, and D. B. Milošević, "High-Order Phase-Dependent Asymmetry in the Above-Threshold Ionization Plateau," Phys. Rev. Lett. **126**(11), 113201 (2021).
22. M. Meckel, D. Comtois, D. Zeidler, A. Staudte, D. Pavičić, H. C. Bandulet, H. Pépin, J. C. Kieffer, R. Dörner, D. M. Villeneuve, and P. B. Corkum, "Laser-induced electron tunneling and diffraction," Science **320**(5882), 1478–1482 (2008).
23. Y. Huismans, A. Rouzée, A. Gijsbertsen, J. H. Jungmann, A. S. Smolkowska, P. S. W. M. Logman, F. Lépine, C. Cauchy, S. Zamith, T. Marchenko, J. M. Bakker, G. Berden, B. Redlich, A. F. G. van der Meer, H. G. Muller, W. Vermin, K. J. Schafer, M. Spanner, M. Yu. Ivanov, O. Smirnova, D. Bauer, S. V. Popruzhenko, and M. J. J. Vrakking, "Time-resolved holography with photoelectrons," Science **331**(6013), 61–64 (2011).

Optics EXPRESS

24. C. I. Blaga, J. Xu, A. D. DiChiara, E. Sistrunk, K. Zhang, P. Agostini, T. A. Miller, L. F. DiMauro, and C. D. Lin, "Imaging ultrafast molecular dynamics with laser-induced electron diffraction," Nature (London) **483**(7388), 194–197 (2012).
25. B. Wolter, M. G. Pullen, A.-T. Le, M. Baudisch, K. Doblhoff-Dier, A. Senftleben, M. Hemmer, C. D. Schröter, J. Ullrich, T. Pfeifer, R. Moshammer, S. Gräfe, O. Vendrell, C. D. Lin, and J. Biegert, "Ultrafast electron diffraction imaging of bond breaking in di-ionized acetylene," Science **354**(6310), 308–312 (2016).
26. W. Becker, S. P. Goreslavski, D. B. Milošević, and G. G. Paulus, "The plateau in above-threshold ionization: the keystone of rescattering physics," J. Phys. B **51**(16), 162002 (2018).
27. C. Figueira de Morisson Faria and A. S. Maxwell, "It is all about phases: Ultrafast holographic photoelectron imaging," Rep. Prog. Phys. **83**(3), 034401 (2020).
28. C. I. Blaga, F. Catoire, P. Colosimo, G. G. Paulus, H. G. Muller, P. Agostini, and L. F. DiMauro, "Strong-field photoionization revisited," Nat. Phys. **5**(5), 335–338 (2009).
29. W. Quan, Z. Lin, M. Wu, H. Kang, H. Liu, X. Liu, J. Chen, J. Liu, X. T. He, S. G. Chen, H. Xiong, L. Guo, H. Xu, Y. Fu, Y. Cheng, and Z. Z. Xu, "Classical Aspects in Above-Threshold Ionization with a Midinfrared Strong Laser Field," Phys. Rev. Lett. **103**(9), 093001 (2009).
30. F. H. M. Faisal, "Ionization surprise," Nat. Phys. **5**(5), 319–320 (2009).